International Journal of Heat and Mass Transfer 53 (2010) 3405–3413

Contents lists available at ScienceDirect

International Journal of Heat and Mass Transfer

journal homepage: www.elsevier.com/locate/ijhmt

The effect of a surfactant monolayer on oxygen transfer across an air/water interface during mixed convection

R.J. Lee, J.R. Saylor *

Clemson University, Department of Mechanical Engineering, Clemson, SC 29634-0921, USA

ARTICLE INFO

Article history:
Received 4 March 2009
Received in revised form 12 March 2010
Accepted 12 March 2010

Keywords:
Gas exchange
Mixed convection
Free surface
Surfactant

ABSTRACT

A set of laboratory experiments are presented that reveal the effect of a surfactant monolayer on the transport of oxygen across an air/water interface during mixed convection conditions. The experiments were conducted in a wind/water tunnel where forced convection was imposed via the air flow, and natural convection by heating the water bulk above the air temperature, resulting in mixed convection conditions. The data acquired during these experiments were used to develop a parameterization between the Sherwood number for oxygen transport *Sh* and the Reynolds *Re* and Rayleigh *Ra* numbers. This parameterization was obtained for the case of a clean water surface and for a water surface covered with a surfactant monolayer. The data reveal that, at a given *Ra* and *Re*, the presence of a surfactant monolayer reduces *Sh* by approximately one order of magnitude. The elasticity of the air/water interface which results from the presence of a surfactant is used to explain these results. The data also show that *Sh* was not sensitive to *Re*. For both the clean and surfactant cases, *Sh* increases with *Ra*.

1. Introduction

The transport of dissolved gases such as oxygen and carbon dioxide across an air/water interface is crucial to the ecology of lakes, streams and oceans. Many factors influence this transport process including wind and the subsurface turbulence generated by wind [1–7], breaking waves and the concomitant effects of bubbles [4,8,5,2,9–11], capillary waves [12,4,8,5,2,13], natural convection [14–16], rain [17,18,7], and chemical reactions within water [19–22], to name just a few.

Existing laboratory and field studies of air/water gas exchange have focused primarily on conditions relevant to air/sea gas exchange, which is to say relatively high wind speeds. When wind speeds are high, forced convection and phenomena such as waves, wave breaking, and the formation of bubbles and drops can dominate air/water gas exchange. The literature on oceanic gas exchange is large and the reader is referred to excellent reviews by Jähne and Haußecker [23], Wanninkhof et al. [24], Frost and Upstill-Goddard [25], and Hasse and Liss [26].

While the globally averaged wind speed over the ocean is ~7 m/s (e.g. Thomas et al. [27]), for lakes, ponds and other small inland water bodies, wind speeds are much smaller. For example, a ten year study by Lenters showed that the average wind speed over Lake Sparkling in the U.S. is 2.3 m/s [28]; Klink [29] showed that for significant portions of the continental United States the average wind speed is less than 3 m/s; and similar results were reported by Deaves and Lines in the United Kingdom [30]. At such low wind speeds, waves, wave breaking and bubble and drop formation become much less relevant, and gas exchange can be dominated by forced convection and/or natural convection, depending on the wind speed and the air-to-water temperature difference. Accordingly, gas exchange at the low wind speeds typical of small lakes is a mixed convection problem where both natural and forced convection play a role. The goal of the present work is to better understand the transport of a dissolved gas, specifically oxygen, during these mixed convection conditions that are relevant to lakes.

To reveal the conditions under which mixed convection conditions exist, a heat transfer/mass transfer analogy is employed to develop an order of magnitude analysis similar to that of Bejan [31] to show where natural and forced convection have comparable contributions to gas exchange. Assuming a mass transfer boundary layer develops on the water-side of the air/water interface, two boundary layer thicknesses can be developed, one for natural convection and one for forced convection. Using the classical laminar flat plate relation:

$$\delta \sim LRe^{-1/2}Sc^{-1/3} \tag{1}$$

a boundary layer thickness for natural convection, can be obtained as:

$$\delta_N \sim LRe_N^{-1/2}Sc^{-1/3} \tag{2}$$

where the characteristic length used for Re_N is the horizontal extent of the water body L (the tank length in this experimental study), and

* Corresponding author. Tel.: +1 864 656 5621; fax: +1 864 656 4435.
E-mail address: jrsaylor@ces.clemson.edu (J.R. Saylor).

0017-9310/$ - see front matter © 2010 Elsevier Ltd. All rights reserved.
doi:10.1016/j.ijheatmasstransfer.2010.03.037

Nomenclature

A	area of water surface
C	oxygen concentration
d	characteristic depth
D	diffusion coefficient
g	gravitational acceleration
H	Henry's law constant
k	mass transfer coefficient
L	characteristic downstream length
$\dot{m}$	mass flow rate
$\dot{m}''$	mass flux
Ra	Rayleigh number
Re	Reynolds number
Sc	Schmidt number
Sh	Sherwood number
u	characteristic velocity
U	wind speed
t	time
T	temperature
V	volume of water tank
Z	difference ratio of mass transfer coefficient

Greek symbols

α	thermal diffusivity
β	coefficient of volumetric expansion
δ	boundary layer thickness
ν	kinematic viscosity
ξ	unheated starting length

Subscripts

0	initial
1	first point of window
3	last point of window
A	air
b	bulk
C	center
d	depth
F	forced convection
G	gas
i	interface
∞	ambient
l	length
L	liquid
M	mass
N	natural convection
s	surface
u	unheated starting length
W	water

the characteristic velocity is based on an order of magnitude analysis for natural convection: [32]

$$u_N = \sqrt{\beta g \Delta T d} \tag{3}$$

where β is the coefficient of volumetric expansion; g, gravitational acceleration; ΔT, the temperature difference between the surface and fluid bulk; and d, the depth of the tank.

The boundary layer thickness for forced convection is:

$$\delta_F \sim L Re_F^{-1/2} Sc^{-1/3} \tag{4}$$

where the characteristic length for Re_F is the same as for Re_N, and the water velocity is taken as 5% of the wind speed [5]. When the ratio δ_F/δ_N is of order unity, mixed convection conditions exist. This ratio is:

$$\frac{\delta_F}{\delta_N} = \frac{Re_N^{1/2}}{Re_F^{1/2}} = \frac{u_N^{1/2}}{u_F^{1/2}} \tag{5}$$

Using water-side properties evaluated at 25 °C when computing the dimensionless quantities, and assuming a characteristic ΔT of 1 K, gives $\delta_F/\delta_N = 5.65$ when $U = 1$ m/s and an extreme value for lake depth of $d = 1000$ m. Keeping the same parameters, but using a shallower depth, $d = 10$ m, more typical of small lakes [16] gives $\delta_F/\delta_N = 1.79$. In both cases, δ_F/δ_N is of order unity. Hence, for wind speeds typical of lakes, gas exchange is a mixed convection problem. For our experimental facility, typical values of ΔT are $\sim$1 K and the maximum wind speed is $U = 4$ m/s. This gives $\delta_F/\delta_N = 0.42$, while at the minimum wind speed of $U = 1$ m/s, $\delta_F/\delta_N = 0.84$, showing that mixed convection conditions exists in our experimental facility as well.

While significant research has been conducted on gas exchange due to natural convection alone, and forced convection alone, few studies have been conducted on gas exchange across an air/water interface during mixed convection. Jähne noted that water that is warmer than the air above it noticeably increases the mass transfer coefficient of CO_2 [33], however the wind speed conditions of this study are unclear. In a field study of the ocean, McNeil and Merlivat observed that natural convection had a significant impact on CO_2 transport at wind speeds of 4–5 m/s, measured 10 m above the ocean surface [14]. Laboratory research performed by Schladow et al. showed that natural convection can increase the mass transfer coefficient of oxygen by 9–40% at a wind speed of 0.1 m/s [15]. Natural convection was shown to have a larger impact on gas exchange at low wind speeds in a study of CO_2 transport in the ocean [34], while a later study suggested that this effect is most important at wind speeds less than 1 m/s [35]. In field research of gas transfer in the ocean, water-side convection at low and moderate wind speeds (<6 m/s) was concluded to be a dominating mechanism controlling the gas transfer of CO_2, as a correlation to only wind speed did not predict gas transfer well [36,37], which was suggested by previous research concerning wind speeds over lakes [38]. An excellent study due to Liss et al. explored the effect of evaporation and condensation on gas exchange in a wind/water tunnel [39]. During the evaporation portion of their experiments, the water temperature was warmer than the air, causing natural convection in the water which occurred in concert with wind speeds ranging from 0.36 to 9.2 m/s. Unfortunately, in an effort to make uniform the oxygen concentration in the water-side of the tank, a recirculation pump was used to mix the water, which most likely masked the natural convection existing in the water and preventing an exploration of mixed convection gas exchange.

The paucity of research on gas exchange across an air/water interface during mixed convection conditions is one of the motivations of the present study. Another important motivation concerns the surface conditions of the air/water interface. In any air/water transport problem, surfactant monolayers can affect the magnitude of transport. Surfactant monolayers are single molecule thick layers that collect at the air/water interface [40]. For the liquid phase surfactants considered here, the monolayer's impact on gas exchange occurs because of its ability to damp subsurface turbulence rather than by creating a barrier through which gas cannot cross or is restricted from crossing [41,42]. When water is subjected to wind stress, surfactants have been shown to decrease the mass transfer due to the damping of subsurface turbulence

[8,43]. Goldman et al. [44] performed experiments using surfactants such as oleyl alcohol and found a 50% decrease in the mass transfer coefficient of oxygen compared to a clean surface for the case of mechanically induced turbulence, a result that they attributed to the damping of subsurface turbulence and reduction in surface renewal by the surfactant. In the research presented here, the effect that oleyl alcohol has on oxygen transport is investigated for mixed convection conditions. This is the first study of its kind that we are aware of.

This study is further motivated by the multiple effects that surfactants can have in this situation. Surfactants restrict motion of the surface fluid at the interface. Hence, mixing of the water bulk will be reduced in the presence of a surfactant, which should result in a reduced oxygen transport rate. However, at the same time, this restriction of surface motion can be expected to result in greater cooling of the water surface. This is because the monolayer, in restricting surface motion, forces surface liquid to be subjected to air cooling for a longer period of time, decreasing the surface temperature, thereby increasing the intensity of natural convection which should increase oxygen transport. This interesting tradeoff further motivates the present study.

In the present work, two surface conditions are considered. First, a water surface covered with a known concentration of the surfactant oleyl alcohol. The second condition is that of a clean water surface, devoid of any surfactant. Such clean water studies are challenging to perform. As demonstrated by Saylor [45], even the most stringent cleaning procedures may result in the formation of a surfactant monolayer which, furthermore, may not be detected by a Wilhelmy plate apparatus. That study revealed that monitoring of the water surface via infrared imaging is needed to ascertain the cleanliness of the water surface. This has been done in the present work, and represents the first study of air/water gas exchange under mixed convection conditions for truly clean surface conditions.

The system considered here consists of an insulated water body with a free water surface in contact with air as illustrated in Fig. 1. The mass flux of oxygen is into the water bulk, and the water temperature is greater than that of the air, creating natural convection conditions within the water. Forced convection also occurs, due to the flow of air over the water surface.

The goal of this work is to develop a relationship between the dimensionless groups relevant to oxygen exchange across the air/water interface: the Reynolds, Rayleigh, and Sherwood numbers. Specifically, the Sherwood number will be parameterized in terms of the Rayleigh and Reynolds numbers:

$$Sh = f(Ra, Re) \tag{6}$$

where Sh is the Sherwood number; Ra, is the Rayleigh number; and Re, is the Reynolds number. These are defined as:

$$Re = \frac{UL}{\nu} \tag{7}$$

$$Ra = \frac{g\beta(T_b - T_s)d^3}{\alpha\nu} \tag{8}$$

$$Sh = \frac{k_L d}{D} \tag{9}$$

where U is the characteristic velocity; L, the characteristic downstream length; ν, the kinematic viscosity of the fluid; g, gravitational acceleration; β, the volume expansion coefficient; T_b, the bulk temperature; T_s, the surface water temperature; d, the characteristic depth; α, the thermal diffusivity of the fluid; k_L the water-side mass transfer coefficient, and D is the diffusion coefficient of oxygen in the fluid [46]. Eqs. (8) and (9) are "water-side" equations meaning that the variables pertain to the water-side of the interface. This is because the resistance to oxygen transport is primarily on the water-side, as is demonstrated below. The Reynolds number is defined in terms of air-side conditions because it is the wind speed that is imposed in these experiments, and the water surface current is a result of that wind speed.

Herein we assume essentially zero resistance to oxygen transport on the air-side of the air/water interface, resulting in the assumed concentration profile presented in Fig. 2 where the profile is vertical on the air-side and there is a finite concentration difference on the water-side. Since conservation of mass requires an equivalence for the mass flux on both sides of the interface, the air-side mass transfer coefficient must approach infinity, $k_G \to \infty$. The validity of the above assumption can be shown using a comparison of the predicted air- and water-side transport coefficients, k_G and k_L, respectively, using a laminar flat plate boundary layer parameterization for Sh [31]:

$$Sh = 0.664 Re^{1/2} Sc^{1/3} \tag{10}$$

where Sc is the Schmidt number, and the water velocity is set to 5% of the air velocity [5]. For the air-side, k_G is obtained from the laminar unheated starting length solution for Sh [46]:

$$Sh_u = Sh_{|\xi=0} \frac{L}{L-\xi}\left[1 - (\xi/L)^{3/4}\right]^{2/3} \tag{11}$$

where ξ is the "unheated length" (the length over which the velocity boundary layer develops, but where mass transfer is not occurring – see Fig. 3), and $Sh_{|\xi=0}$ is the Sherwood number for the case

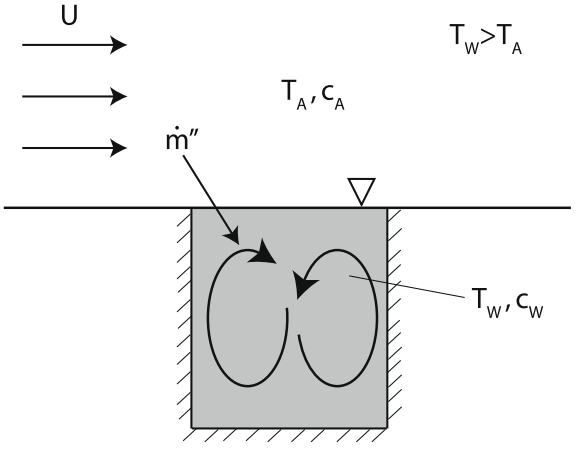

Fig. 1. Illustration of system under consideration.

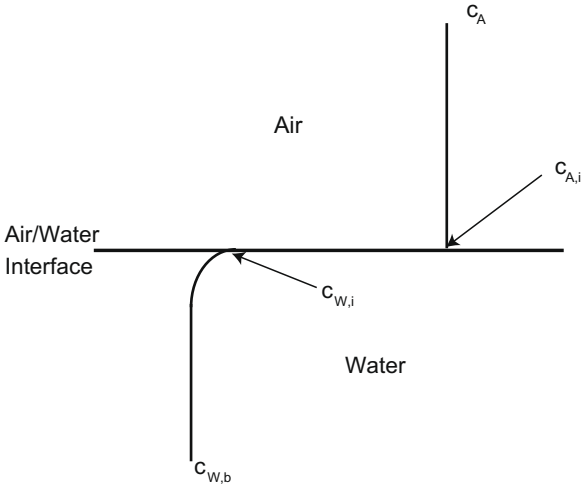

Fig. 2. Illustration of assumed concentration profiles.

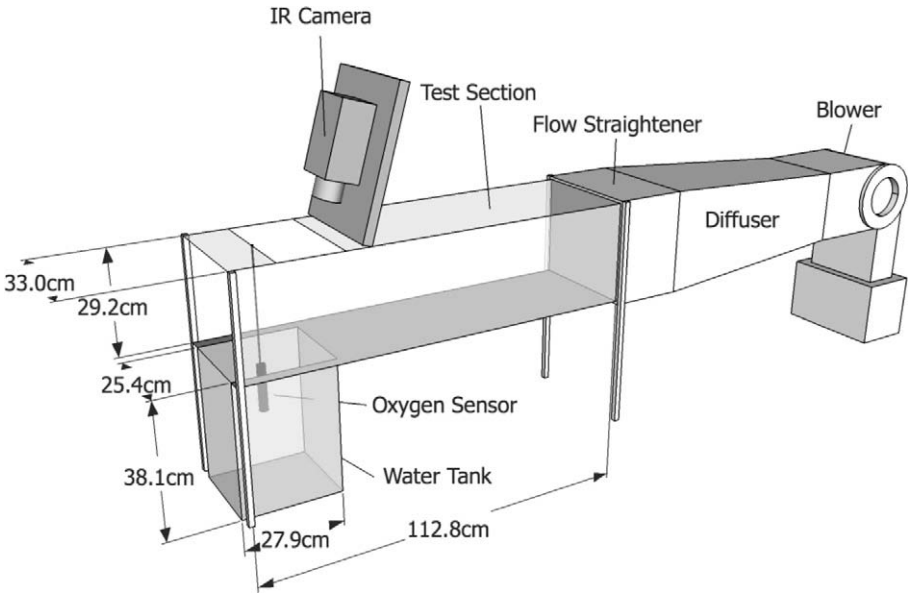

Fig. 3. Experimental apparatus showing wind/water tunnel and measuring equipment.

where the velocity and mass transfer boundary layers develop from the same starting point (Eq. (10)). Using Eqs. (10) and (11), values for k_G and k_L were obtained using the parameters presented in Table 1. The characteristic length used for *Re* and *Sh* was $L = 27.9$ cm for the experimental facility on the water-side. On the air-side of the experimental facility, $L = 114.9$ cm, and $\xi = 86.4$ cm. Using Eq. (10) to obtain *Sh* on the water-side and Eq. (11) to obtain *Sh* on the air-side and then obtaining the mass transfer coefficients gave $k_L = 8.8 \times 10^{-6}$ m/s and $k_G = 0.008$ m/s. Hence the air-side mass transfer coefficient is about three orders of magnitude greater than that on the water-side, justifying the assumptions described above.

2. Experimental method

Experiments were conducted in the wind/water tunnel illustrated in Fig. 3. The wind tunnel consists of a radial blower, diffuser, flow straightener, and test section. The water tank is 38.1 cm $D \times$ 27.9 cm $L \times$ 25.4 cm W and insulated with two layers of 1.9 cm thick polystyrene. In order to calculate an average surface temperature (T_s in Eq. (8)), a ThermaCAM^{TM} SC1000 infrared camera was used to capture the surface temperature field. A single value for T_s was obtained from each image by averaging over all pixels, excluding those corresponding to the tank walls, bad pixels, and the oxygen sensor wire (see Fig. 4, below). The infrared camera was mounted above the test section of the wind tunnel with the lens located 86.4 cm from the water surface and positioned 16° from vertical so the camera did not image a thermal reflection of itself. The camera has a resolution of ±0.07 °C and an accuracy of ±2%. The water bulk oxygen concentration and temperature were measured using a Hach HQ30 oxygen sensor with an integrated thermistor. The sensor was positioned in the geometric center of the tank; it was assumed that the bulk water was well-mixed and therefore a single measurement was used to characterize the bulk temperature and oxygen concentration. The wire connecting the oxygen probe to the data logger hung in the middle of the test section of the wind tunnel. Examination of the infrared (IR) images attained from the IR camera revealed no visible disruption of the surface flow due to the wire (e.g. Fig. 5). The oxygen sensor has a resolution of ±0.1 mg/L and an accuracy of ±0.2 mg/L, while the integrated thermistor has a resolution of ±0.1 °C and accuracy of ±0.3 °C.

Table 1
Parameters for air-side and water-side mass transfer coefficient comparison.

Parameter	Air-side	Water-side
Wind speed (m/s)	4	0.2
ν (m^2/s)	1.5×10^{-5}	8.94×10^{-7}
Sc	0.75	356
D (m^2/s)	2.1×10^{-5}	2.1×10^{-9}

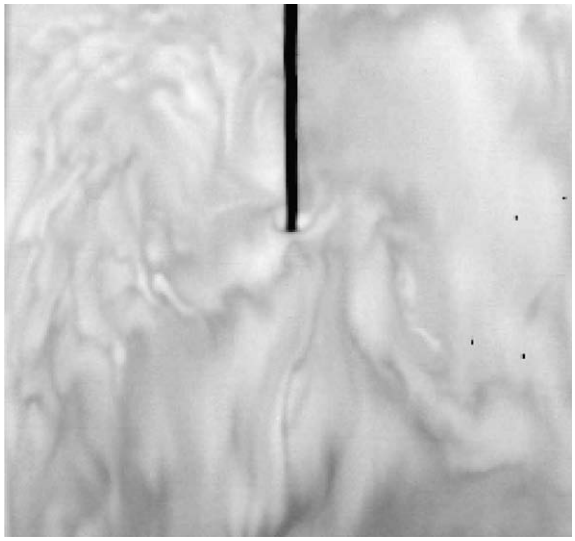

Fig. 4. Surface temperature field of a surfactant covered water surface obtained from an IR image of a tap water experiment. The wind speed is $U = 3$ m/s, and the wind direction is from bottom to top. The black line in the upper middle portion of the image is the oxygen sensor wire.

A total of three surface conditions were explored: oleyl alcohol (controlled surfactant), tap (indigenous surfactant), and clean. For the oleyl alcohol case, oleyl alcohol was applied to the surface of filtered tap water. For the tap water case, filtered tap water was used, which had indigenous surfactants on the surface. The clean surface case was created using tap water cleaned using a method described later in this section. Wind speeds from 0 to 4 m/s were

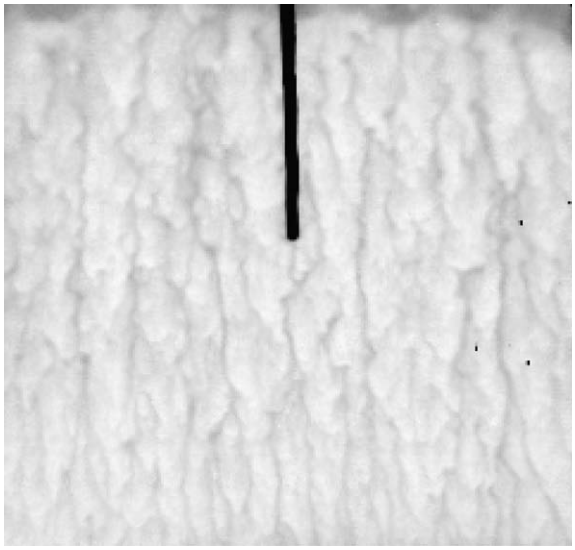

Fig. 5. Surface temperature field of a clean water surface obtained from an IR image. The wind speed is $U = 3$ m/s, and the wind direction is from bottom to top. The black line in the upper middle portion of the image is the oxygen sensor wire.

investigated for the oleyl alcohol and tap water cases in increments of 1 m/s, and wind speeds of 1–4 m/s were investigated for the clean surface case, also in increments of 1 m/s. The wind speed was characterized by an average of 9 wind speed measurements taken by an anemometer at locations uniformly spaced across the cross-section of the wind tunnel test section.

Water heated to a temperature greater than that of air was used to cause natural convection. Initial starting temperatures in the water bulk ranged from 30 to 48 °C for all surface conditions. These temperatures are all much warmer than the air temperature, normally around 23 °C. Both hot tap water and/or an immersion heater were used to attain the desired starting temperature. For all experiments, once the starting temperature was attained, the water was allowed to cool naturally for the duration of the run. Clean surface runs were 15 min in duration, oleyl runs were 1 h in duration, and tap runs were 8 h in duration. The reason for the differences in duration is discussed later in this section.

Surface cleanliness was determined by examination of the IR images using the method described by Saylor [45] who showed that the presence of surfactant monolayers can be detected by the change in length scales observed in IR images. A sample IR image of a water surface covered with a surfactant monolayer is presented in Fig. 4, and an image of a completely clean surface is presented in Fig. 5. The clean surface is characterized by finer scale structures compared to the surfactant covered surface. In both of these images, bad pixels can be observed (unresponsive pixels that appear black); however, these were not used in calculation of T_s. The wire connecting the oxygen probe to the data logging unit can be seen in all images; as noted above, this part of the image was not used in calculation of T_s either.

Uniform surfactant coverage was required for the oleyl alcohol experiments. To minimize the formation of a Reynolds ridge [47–49], the equilibrium spreading pressure, Π^e [50] was imposed on the water surface. This pressure is achieved when an excess of the surfactant is present on the surface. To attain Π^e, a solution of oleyl alcohol in heptane was created, where heptane was used as a spreading agent for the oleyl alcohol to ensure that the surfactant covered the entire water surface. In addition to this, oleyl alcohol was placed in a reservoir located in the downstream corner of the tank, at the water surface. In this way, any loss of oleyl alcohol that might have occurred (due to evaporation, for example) was replaced via spontaneous spreading from this reservoir. The equilibrium spreading pressure of oleyl alcohol at 25 °C is $\Pi^e = 30.5$ dyne/cm and has a surface concentration of $c = 0.147$ μg/cm^2 [51], which was therefore the concentration for all of the oleyl alcohol experiments presented here. Oleyl alcohol was added to the reservoir every 20 min after the initial application to insure that the reservoir remained full and that there was complete surfactant coverage for the entire experiment.

To create clean water surfaces, the method of Kou and Saylor [52] was used. Here the water was first cleaned by bubble sparging, and then swiped. Subsequent to this, a rake consisting of microbore tubes was precisely located at the air/water interface, at the downstream end of the tank. Suction applied to the tube rake was used to remove surfactants from the water surface. This method takes advantage of the tendency of the wind to blow surfactants to the downstream edge of the tank where the rake was located. Since wind stress was required for this apparatus to function well, 0 m/s experiments are not presented here for the clean surface condition. The tap water case was achieved by simply using tap water without any cleaning, since surfactants indigenous to tap water completely covered the water surface.

The oxygen concentration difference between the water and the air was created by sparging the water bulk with N_2 for approximately 40 min before the beginning of each run, thereby removing oxygen from the water. Once the experiments were initiated, oxygen was transferred from the air to the water. Experimental runs were 1 h for the oleyl alcohol case, 8 h in duration for the tap case, and 15 min each for the clean surface case. Clean surface runs were shorter because the surfactant removal method described above no longer functioned properly when the water level fell beneath the tank rim. Because the tube rake removed a small amount of water in the process of removing surfactants, the water surface was lowered and surface cleaning ceased after about 15 min, at which point data acquisition was stopped. For a typical tap water run, the initial starting temperature was 42 °C. A typical clean surface or oleyl alcohol run began at a specified temperature, anywhere from 30 to 48 °C. The 8 h duration of the tap experiments allowed all runs to be started at the same temperature, since a satisfactory decrease in temperature occurred over that period. Oleyl alcohol runs were shorter due to the required periodic addition of oleyl alcohol to the surfactant reservoir.

The mass transfer coefficient is defined as:

$$k_L = \frac{\dot{m}}{A(\frac{C_A}{H} - C_W)} \tag{12}$$

where C_W is the oxygen concentration in the water bulk; C_A, the concentration of oxygen in air (assumed to be constant); A, the area of the water surface; and $\dot{m}$, the mass transfer rate. The ratio of concentration of oxygen in the air, C_A, to the Henry's law constant, H, is equivalent to the concentration of oxygen on the water-side of the air/water interface $C_{W,i}$, i.e. $\frac{C_A}{H} = C_{W,i}$, which is assumed to be at solubility. The solubility data used to calculate $C_{W,i}$ (or $\frac{C_A}{H}$) was obtained from Tchobanoglous et al. [53] and varies with both temperature and barometric pressure. The barometric pressure data used to calculate $C_{W,i}$ was taken from the average pressure reported by the Clemson University Department of Entomology, Soils, and Plant Sciences weather station for each day that an experiment was run, while the temperature data was taken from the average water surface temperature T_s. The mass transfer rate can be written as:

$$\frac{\dot{m}}{V} = \frac{d\left(\frac{C_A}{H} - C_W\right)}{dt} = k_L \frac{A}{V}\left(\frac{C_A}{H} - C_W\right) \tag{13}$$

where V is the volume of water in the tank and t is time. Hence, k_L can be expressed as:

$$k_L = -\frac{V}{A}\frac{\frac{d(\frac{C_A}{H}-C_W)}{dt}}{\frac{C_A}{H}-C_W} \tag{14}$$

Separating variables, integrating, and reducing $\frac{V}{A}$ to d gives:

$$\left(\frac{k_L}{d}\right)t = -\ln\left(\frac{\frac{C_A}{H}-C_W}{\frac{C_A}{H}-C_{W,0}}\right) \tag{15}$$

where $C_{W,0}$ is the initial oxygen concentration in the water bulk. For a constant mass transfer coefficient, $\left(\frac{C_A}{H}-C_w\right)$ decays exponentially resulting in a linear plot of $\ln\left(\frac{\frac{C_A}{H}-C_W}{\frac{C_A}{H}-C_{W,0}}\right)$ versus time. A sample time trace is presented in Fig. 6 showing linear behavior for $\ln\left(\frac{\frac{C_A}{H}-C_W}{\frac{C_A}{H}-C_{W,0}}\right)$, and therefore constant k_L for this run. In this work, k_L was computed by obtaining linear fits to the acquired data (as is done in Fig. 6), and obtaining k_L/d from the slope of the fits.

The procedure detailed above was acceptable for the relatively short 15 min clean surface runs, where the assumption of constant k_L was appropriate. However, the tap runs were 8 h in duration and oleyl runs 1 h in duration, and hence the assumption of quasi-steady state was not valid. During this period of time, significant changes in the water temperature occurred, resulting in changes in Ra, and hence in k_L, thereby invalidating the assumption of exponential decay. To address this, a sliding window of variable size was applied to the raw data. At each point in the time trace, a value of k_L was computed using just the data in the window surrounding that point and assuming exponential decay in that subset of the overall time trace. The window was slid over the T_s time trace, resulting in a value for k_L at each point in that time trace. Because the temperature decreased continuously during the course of the experiment, some degree of error exists for any finite window size used since H must be evaluated at a single temperature. This error is quantified as:

$$Z = \frac{k_1 - k_3}{k_C} \tag{16}$$

where k_1 is the mass transfer coefficient with H evaluated at the maximum T_s in the window; k_3, the mass transfer coefficient with H evaluated at the minimum T_s in the window; and k_C, the mass transfer coefficient with H evaluated at T_s in the center of the window. For each point in the time trace, the window size was iteratively adjusted until $Z = 0.045$, and then k_L was computed. This procedure insured that all values of k_L had the same (4.5%) error. This would not have been the case using a fixed window size, since the variation in T_s for a fixed sized window decreases as the rate of tank cooling decreases. The choice of $Z = 0.045$ was somewhat arbitrary; smaller values of Z yielded very noisy time traces of k_L, and larger values of Z blurred the long time behavior of k_L. Though a Z value was not imposed for the clean surface data, it was calculated for each experiment and varied from 0.96% to 9.1%. Although it would be desirable to have the same value of Z for the clean, oleyl, and tap experiments, the short duration of the clean surface time traces restricted this approach.

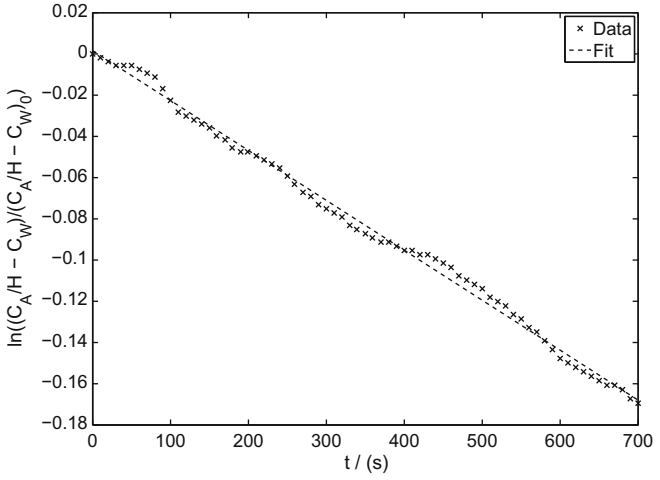

Fig. 6. Time trace of log of concentration ratio for a clean surface run. The slope of this line is used to calculate k_L.

3. Results

A plot of Sh versus Ra is presented in Fig. 7 for all of the clean and oleyl alcohol runs and for all wind speeds investigated. At a given Ra, the oleyl data and clean surface data are separated by nearly an order of magnitude in Sherwood number. These two data sets are each well-fit by a single power law expressing Sh in terms of Ra without employing Re, *viz.* these gas exchange results show little dependence on wind speed. The power law fit for the oleyl data is:

$$Sh = 354.7Ra^{0.2475} \tag{17}$$

while the power law fit for the clean surface data is

$$Sh = 1.202 \times 10^{-6}Ra^{1.302} \tag{18}$$

These two power laws differ significantly: the exponent is a factor of 5 larger for the clean surface case and the prefactors differ by 8 orders or magnitude. Careful examination of the clean surface data presented in Fig. 7 reveals that the $U = 1$ m/s points cluster beneath the fit and do not appear as well-fit by the power law as for the other wind speeds. This can be explained by the fact that for these runs complete elimination of the surfactant monolayer, as described in Section 2, did not occur. Typically about 3 cm remained on the downstream end of the tank. It is likely that this caused these 1 m/s data points to drop below the fit (and, as expected, closer to the oleyl data).

For the clean surface data, the uncertainty in Ra is $\pm 9.66 \times 10^8$, the uncertainty in Sh is $\pm 6.42 \times 10^6$, and the applicability bounds of the fit using a 95% confidence interval is $\log(Sh) = \pm 0.5983$. For oleyl data, the uncertainty in Ra is $\pm 5.69 \times 10^8$, the uncertainty in Sh is $\pm 1.54 \times 10^3$ and the range of applicability of the fit using a 95% confidence interval is $\log(Sh) = \pm 0.0984$.

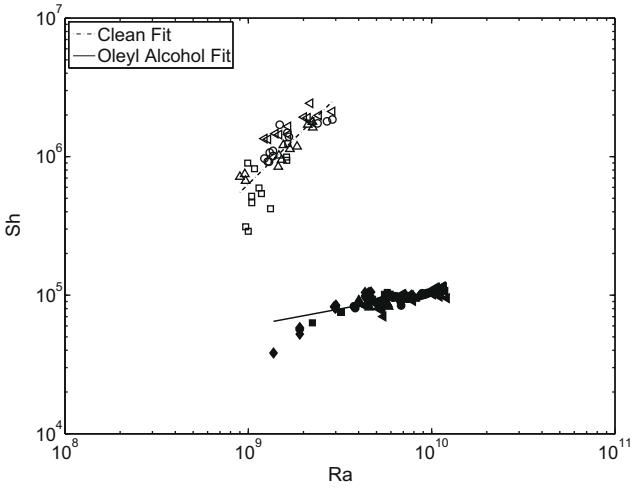

Fig. 7. Sherwood–Rayleigh plot of oleyl alcohol (♦0 m/s, ■ 1 m/s, ▲ 2 m/s, •3 m/s, ◄ 4 m/s), and clean surface (□ 1 m/s, △ 2 m/s, ○ 3 m/s, ◁ 4 m/s), data and fits. Every 20th oleyl data point is shown.

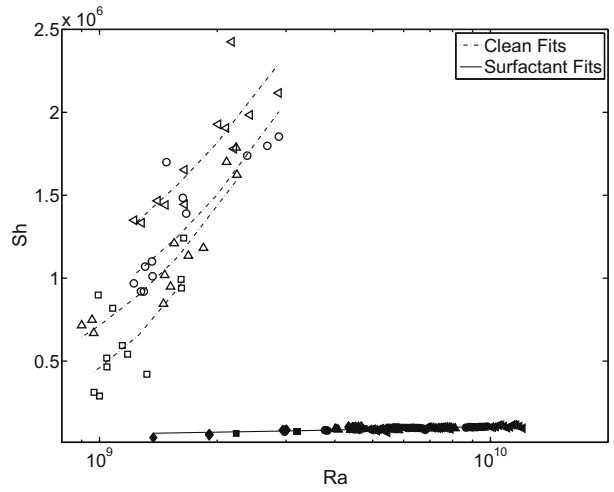

Fig. 8. Sherwood–Rayleigh plot of oleyl alcohol (♦0 m/s, ■ 1 m/s, ▲ 2 m/s, •3 m/s, ◄ 4 m/s), and clean surface (□ 1 m/s, △ 2 m/s, ○ 3 m/s, ◁ 4 m/s), data and fits. Every 20th oleyl data point is shown.

The clean surface data and oleyl data are replotted on semi-log coordinates in Fig. 8. Individual fits are provided for each wind speed. This plot shows that the oleyl data is much less wind speed dependent compared to the clean surface data. Indeed, an increase in *Sh* with wind speed seems to exist in Fig. 8 for the clean case. However, no statistically significant separation was found in the fits for each wind speed using a 95% confidence interval for this clean surface condition.

A plot of *Sh* versus *Ra* for oleyl alcohol and tap water data can be seen in Fig. 9. The data reveals that the tap water case does not differ in behavior from the oleyl alcohol covered surface. Computational work due to Handler et al. [54] may explain the similarity in the behavior of the oleyl alcohol and tap water data presented here. In their work, direct numerical simulations of a vortex pair impinging on a free surface from below were investigated for several values of the Marangoni number *Ma*, defined as

$$Ma = -\frac{\partial\sigma}{\partial c}\frac{c}{\sigma} \tag{19}$$

where σ is the surface tension at a surfactant concentration c. These simulations showed that, for $Ma > 10^{-2}$, the dynamics of the subsurface hydrodynamics are virtually identical to those of a surface having a no-slip boundary condition (*viz.* a solid wall), and behavior similar to a completely clean surface is not observed until $Ma < 10^{-4}$. For oleyl alcohol at the concentration $c = 0.147\ \mu g/cm^2$ explored here, *Ma* is significantly above the 10^{-2} value where Handler et al. [54] found that no-slip behavior is a reasonable approximation. Although it cannot be demonstrated, it is possible that the same was true for the tap case, *viz.* both surfactant cases considered here gave behavior reasonably close to that of a no-slip boundary condition. Further studies would be needed to demonstrate this conclusively.

In applications, one is often more interested in actual mass fluxes and temperature differences, rather than the dimensionless groups, *Sh* and *Ra*. To reveal trends in these terms, a plot is presented in Fig. 10 of the oxygen mass flux versus the bulk water to air temperature difference $T_b - T_\infty$. This plot shows that, for all wind speeds, the clean surface data gives significantly larger mass fluxes than its oleyl counterpart for all $T_b - T_\infty$. There also appears

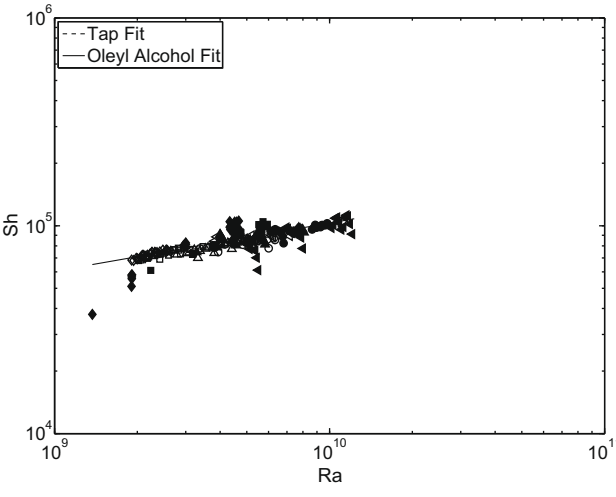

Fig. 9. Sherwood–Rayleigh plot of oleyl alcohol (♦0 m/s, ■ 1 m/s, ▲ 2 m/s, •3 m/s, ◄ 4 m/s), and tap water (◇ 0 m/s, □ 1 m/s, △ 2 m/s, ○ 3 m/s, ◁ 4 m/s), data and fits. For clarity, every 20th oleyl and every 500th tap water data point is shown.

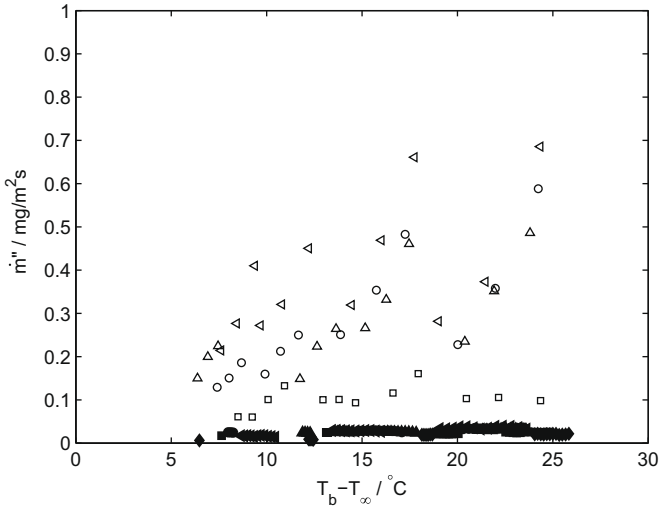

Fig. 10. Plot of mass flux of oxygen and overall temperature difference between water bulk and air temperature for oleyl alcohol (♦0 m/s, ■ 1 m/s, ▲ 2 m/s, •3 m/s, ◄ 4 m/s) and clean surface (□ 1 m/s, △ 2 m/s, ○ 3 m/s, ◁ 4 m/s) data. Every 20th oleyl data point is shown for clarity.

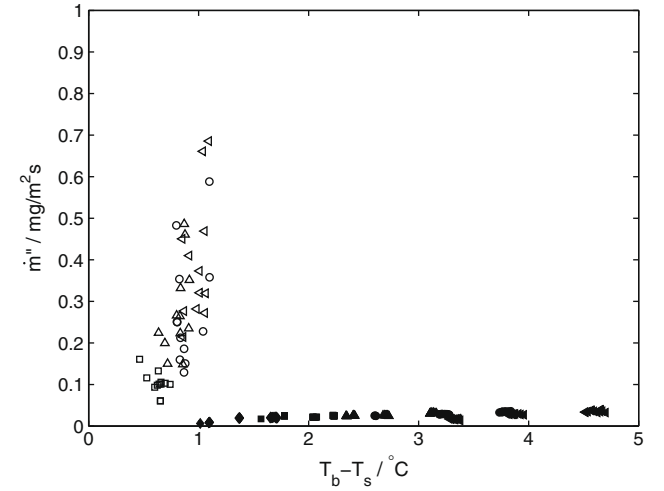

Fig. 11. Plot of mass flux of oxygen and water-side temperature difference ($T_b - T_s$) for oleyl alcohol (♦0 m/s, ■ 1 m/s, ▲ 2 m/s, •3 m/s, ◄ 4 m/s) and clean surface (□ 1 m/s, △ 2 m/s, ○ 3 m/s, ◁ 4 m/s) conditions. Every 20th oleyl data point is shown for sake of clarity.

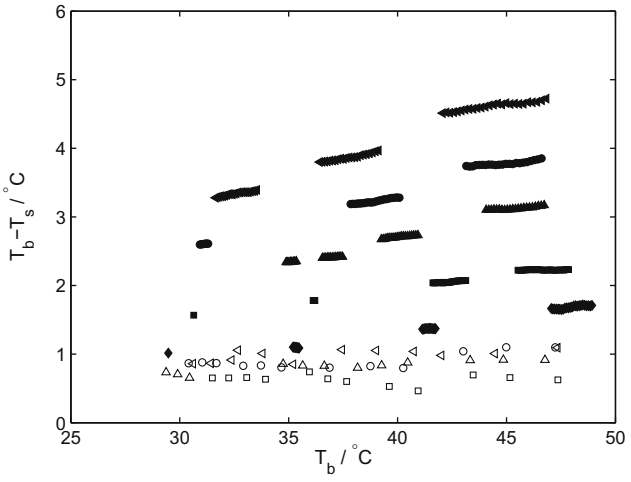

Fig. 12. Plot of $T_b - T_s$ against T_b for oleyl alcohol (♦0 m/s, ■ 1 m/s, ▲ 2 m/s, •3 m/s, ◄ 4 m/s) and clean surface (□ 1 m/s, △ 2 m/s, ○ 3 m/s, ◁ 4 m/s) data. Every 20th oleyl data point is shown.

to be a general trend of increasing mass flux with wind speed for the clean surface case, though there is no such behavior for the oleyl case. These mass flux data are replotted in Fig. 11 in terms of oxygen mass flux versus the bulk to surface temperature difference $T_b - T_s$. This plot results in a partial collapse of the clean surface data set, not seen in Fig. 10. That is, when plotted in this way, the wind speed sensitivity for the clean surface data is essentially eliminated. This plot also shows much larger mass fluxes for the clean surface case.

The range in $T_b - T_s$ is much larger for the oleyl case than for the clean case in Fig. 11 in spite of the fact that the range in $T_b - T_\infty$ is very similar for both cases, as evidenced by Fig. 10. This point is further explored in Fig. 12 where $T_b - T_s$ is plotted against T_b (since T_∞ is essentially constant, plotting against T_b instead of $T_b - T_\infty$ results only in a shift of the x-axis) for the clean surface and oleyl cases. The oleyl data show an increase in $T_b - T_s$ with T_b, particularly at the higher wind speeds that is not seen for the clean surface data. Also, $T_b - T_s$ increases with wind speed to a greater extent for the oleyl case than for the clean surface case. This plot reveals, among other things, that the water surface is more effectively cooled by the wind when the surface is covered with a surfactant monolayer, and that without such a monolayer, increasing the wind speed does little to cool that surface.

4. Discussion

The main result of these experiments can be seen in Fig. 7 which shows that the removal of a surfactant monolayer from a water surface results in a one order of magnitude increase in the Sherwood number for oxygen transfer, at a given value of *Ra*. Since k_L is essentially the only variable in *Sh* that changes in these experiments (Eq. (9)), this result shows that the presence of a surfactant significantly reduces the mass transfer coefficient. This point is revealed in a different way in Fig. 11, where the mass flux is shown to be dramatically reduced in the presence of a surfactant monolayer at any given value of $T_b - T_s$. The power law fits of *Sh* to *Ra* presented in Eqs. (17) and (18) for the oleyl and clean data sets, respectively, show that the surfactant reduces the overall magnitude of the gas exchange, and the rate at which *Sh* increases with *Ra*. These are the first results of their kind, obtained for mixed convection conditions.

As noted in Section 1, the resistance to gas exchange exists almost exclusively on the water-side of the air/water interface. Hence, transport will be determined by the degree to which the water-side turbulence reduces the boundary layer thickness. Surfactant monolayers impart elasticity to the water surface [55,50] reducing the ability of subsurface motions to penetrate to the interface, thereby impeding transport. This mechanism is clearly at play in these experiments, where we see dramatic reductions in the Sherwood number and in the mass flux when a surfactant monolayer is present.

The analysis provided above does not, however, provide a complete picture of the transport processes. It is true that the elasticity of a monolayer can, and does, reduce transport. However, as shown in Fig. 12, for the surfactant case, $T_b - T_s$ is larger at a given value of T_b than for the clean case, and $T_b - T_s$ increases more with wind speed than for the clean case. Since *Ra* is proportional to $T_b - T_s$ (Eq. (8)) this means that the presence of a surfactant increases the Rayleigh number (for a given T_b), and hence increases natural convection motion. It could be argued, therefore, that the presence of a monolayer, while reducing transport by suppressing turbulence near the interface, may also *increase* transport by increasing the intensity of natural convection. Stated in another way, at a given value of T_b, and at a given wind speed, the deposition of a surfactant monolayer will serve to increase $T_b - T_s$ and *Ra*. This does indeed occur, however this effect is a minority player as can be seen in Fig. 7 which shows that for the entire range of *Ra* explored here, the values of *Sh* for oleyl alcohol are much smaller than those for the clean case, even though the range in T_b is about the same for these two cases. Hence, adding a surfactant will increase the natural convection, but this effect does not compete with the damping of subsurface turbulence that also occurs with the deposition of the monolayer.

Fig. 7 also shows that gas exchange shows little sensitivity to wind speed, for the conditions explored here. This is not surprising for the oleyl case where the monolayer restricts motion at the air/water interface and, therefore, reduces the impact of forced convection induced by shear imposed on the air-side of the interface. However, for the clean case, one might expect that the lack of surfactants would result in an increasing degree of mixing of the water and therefore gas exchange, with wind speed. This effect does not seem to dominate, however, and there is only a slight wind-speed sensitivity apparent in the clean surface data (Figs. 7 and 8), and this difference is not statistically significant. However, it is greater than for the surfactant case shown in Fig. 8.

It is noted that these results were obtained for a fixed size water surface and a fixed upstream region over which the air-side boundary layer develops. Variation of these parameters could change the results obtained here.

5. Conclusion

The effect of surfactants on gas exchange were observed under the condition of mixed convection. A parameterization of *Sh* in terms of *Ra* was obtained for clean surface, oleyl alcohol, and tap water conditions. The original goal was to parameterize *Sh* in terms of *Ra* and *Re*, however *Sh* was found to be essentially insensitive to wind speed for the conditions investigated here. The results showed that gas exchange is much more effective with a clean water surface than a surfactant covered one. The clean surface data also revealed much greater sensitivity of *Sh* to *Ra* than for the surfactant-covered case. The cause for these differences can be attributed to the elasticity imparted to the air/water interface by a surfactant monolayer. On the water-side of the interface, the surfactant reduces the subsurface turbulence, which in turn reduces mixing from the water surface to the bulk.

Acknowledgment

Support from the National Science Foundation is gratefully acknowledged.

References

[1] P.S. Liss, A.L. Chuck, S.M. Turner, A.J. Watson, Air–sea gas exchange in Antarctic waters, Antarctic Sci. 16 (2004) 517–529.
[2] F.J. Ocampo-Torres, M.A. Donelan, N. Merzi, F. Jia, Laboratory measurements of mass transfer of carbon dioxide and water vapour for smooth and rough flow conditions, Tellus 46 (1994) 16–32.
[3] J.J. Cole, J.F. Caraco, Atmospheric exchange of carbon dioxide in a low-wind oligotrophic lake measured by the addition of SF_6, Limnol. Oceanogr. 43 (1998) 647–656.
[4] Y. Cohen, W. Cocchio, D. Mackay, Laboratory study of liquid-phase controlled volatilization rates in presence of wind waves, Environ. Sci. Technol. 12 (1978) 553–558.
[5] B. Jähne, K.O. Münnich, U. Siegenthaler, Measurements of gas exchange and momentum transfer in a circular wind–water tunnel, Tellus 31 (1979) 321–329.
[6] C.R. Chu, G.H. Jirka, Wind and stream flow induced reaeration, J. Environ. Eng. 129 (2003) 1129–1136.
[7] D.T. Ho, F. Veron, E. Harrison, L.F. Bliven, N. Scott, W.R. McGillis, The combined effect of rain and wind on air–water gas exchange: a feasibility study, J. Mar. Syst. 66 (2007) 150–160.
[8] H.C. Broecker, J. Petermann, W. Siems, The influence of wind on CO_2-exchange in a wind-wave tunnel, including the effects of monolayers, J. Mar. Res. 36 (1978) 595–610.
[9] W.E. Asher, L.M. Karle, B.J. Higgins, P.J. Farley, E.C. Monahan, I.S. Leifer, The influence of bubble plumes on air–seawater gas transfer velocities, J. Geophys. Res. 101 (1996) 12027–12041.
[10] W.E. Asher, L.M. Karle, B.J. Higgins, On the differences between bubble-mediated air–water transfer in freshwater and seawater, J. Mar. Res. 55 (1997) 813–845.
[11] E.J. Boettcher, J. Fineberg, D.P. Lathrop, Turbulence and wave breaking effects on air–water gas exchange, Phys. Rev. Lett. 85 (2000) 2030–2033.
[12] G.M. Hidy, E.J. Plate, Wind action on water standing in a laboratory channel, J. Fluid Mech. 26 (1966) 651–687.
[13] J.R. Saylor, R.A. Handler, Capillary wave gas exchange in the presence of surfactants, Exp. Fluids 27 (1999) 332–338.
[14] C.L. McNeil, L. Merlivat, The warm oceanic surface layer: implications for CO_2 fluxes and surface gas measurements, Geophys. Res. Lett. 23 (1996) 3575–3578.
[15] S.G. Schladow, M. Lee, B.E. Hürzeler, P.B. Kelly, Oxygen transfer across the air–water interface by natural convection in lakes, Limnol. Oceanogr. 47 (2002) 1394–1404.
[16] W. Eugster, G. Kling, T. Jonas, J.P. McFadden, A. Wüest, S. MacIntyre, F.S. Chapin, CO_2 exchange between air and water in an Arctic Alaskan and midlatitude Swiss lake: importance of convective mixing, J. Geophys. Res. 108 (2003) 4362.
[17] D.T. Ho, L.F. Bliven, R. Wanninkhof, P. Schlosser, The effect of rain on air–water gas exchange, Tellus 49 (1997) 149–158.
[18] D.T. Ho, W.E. Asher, L.F. Bliven, P. Schlosser, E.L. Gordan, On mechanisms of rain-induced air–water gas exchange, J. Geophys. Res. 105 (2000) 24045–24057.
[19] C. Yin, J. Hassett, Gas-partitioning approach for laboratory and field studies of mirex fugacity, Environ. Sci. Technol. 20 (1986) 1213–1217.
[20] C. Yin, J.P. Hassett, Fugacity and phase distribution of mirex in Oswego River and Lake Ontario waters, Chemosphere 19 (1989) 1289–1296.
[21] R. Wanninkhof, Relationship between gas exchange and wind speed over the ocean, J. Geophys. Res. 97 (1992) 7373–7381.
[22] R. Wanninkhof, M. Knox, Chemical enhancement of CO_2 exchange in natural waters, Limnol. Oceanogr. 41 (1996) 689–697.
[23] B. Jähne, H. Haußecker, Air–water gas exchange, Ann. Rev. Fluid Mech. 30 (1998) 443–468.
[24] R. Wanninkhof, W.E. Asher, D.T. Ho, C. Sweeney, W.R. McGillis, Advances in quantifying air–sea gas exchange and environmental forcing, Annu. Rev. Mar. Sci. 1 (2009) 213–244.
[25] T. Frost, R.C. Upstill-Goddard, Air–sea gas exchange into the millennium: progress and uncertainties, Oceanogr. Mar. Biol. 37 (1999) 1–45.
[26] L. Hasse, P.S. Liss, Gas-exchange across the air–sea interface, Tellus 32 (1980) 470–481.
[27] B.R. Thomas, E.C. Kent, V.R. Swail, D.I. Berry, Trends in ship wind speeds adjusted for observation method and height, Int. J. Climatol. 28 (2008) 747–767.
[28] J.D. Lenters, T.K. Kratz, C.J. Bowser, Effects of climate variability on lake evaporation: results from a long-term energy budget study of Sparkling Lake, northern Wisconsin (USA), J. Hydrol. 308 (2005) 168–195.
[29] K. Klink, Climatological mean and interannual variance of United States surface wind speed, direction and velocity, Int. J. Climatol. 19 (1999) 471–488.
[30] D.M. Deaves, I.G. Lines, The nature and frequency of low wind speed conditions, J. Wind Eng. 73 (1998) 1–29.
[31] A. Bejan, Convection Heat Transfer, second ed., John Wiley & Sons, Inc., 1995.
[32] P.H. Oosthuizen, D. Naylor, Introduction to Convective Heat Transfer Analysis, McGraw-Hill, New York, 1999.
[33] B. Jähne, K.O. Münnich, R. Bösinger, A. Dutzi, W. Huber, P. Libner, On the parameters influencing air–water gas exchange, J. Geophys. Res. 92 (1987) 1937–1949.
[34] B. Ward, R. Wanninkhof, W.R. McGillis, A.T. Jessup, M.D. DeGrandpre, J.E. Hare, J.B. Edson, Biases in the air–sea flux of CO_2 resulting from ocean surface temperature gradients, J. Geophys. Res. 109 (2004) C08S08.
[35] C. Zülicke, Air–sea fluxes including the effect of the molecular skin layer, Deep Sea Res. II 52 (2005) 1220–1245.
[36] N.M. Frew, E.J. Bock, U. Schimpf, T. Hara, H. Haußecker, J.B. Edson, W.R. McGillis, R.K. Nelson, S.P. McKenna, B.M. Uz, B. Jähne, Air–sea gas transfer: its dependence on wind stress, small-scale roughness, and surface films, J. Geophys. Res. 109 (2004) C08S17, doi:10.1029/2003JC002131.
[37] C.D. Jeffery, D.K. Woolf, I.S. Robinson, C.J. Donlon, One-dimensional modelling of convective CO_2 exchange in the Tropical Atlantic, Ocean Model. 19 (2007) 161–182.
[38] J. Crusius, R. Wanninkhof, Gas transfer velocities measured at low wind speed over a lake, Limnol. Oceanogr. 48 (2003) 1010–1017.
[39] P.S. Liss, P. Balls, F.N. Martinelli, M. Coantic, The effect of evaporation and condensation on gas transfer across an air–water interface, Oceanol. Acta 4 (1981) 129–138.
[40] G.T. Barnes, I.R. Gentle, Interfacial Science: An Introduction, first ed., Oxford University Press, 2005.
[41] N.M. Frew, J.C. Goldman, M.R. Dennett, A.S. Johnson, Impact of phytoplankton-generated surfactants on air–sea gas-exchange, J. Geophys. Res. Oceans 95 (1990) 3337–3352.
[42] W.E. Asher, J.F. Pankow, Prediction of gas/water mass transport coefficients by a surface renewal model, Environ. Sci. Technol. 25 (1991) 1294–1300.
[43] S.P. McKenna, W.R. McGillis, The role of free-surface turbulence and surfactants in air–water gas transfer, Int. J. Heat Mass Transfer 47 (2004) 539–553.
[44] J.C. Goldman, M.R. Dennett, N.M. Frew, Surfactant effects on air–sea gas-exchange under turbulent conditions, Deep Sea Res. 35 (1988) 1953–1970.
[45] J.R. Saylor, Determining liquid substrate cleanliness using infrared imaging, Rev. Sci. Instrum. 72 (2001) 4408–4414.
[46] F.P. Incropera, D.P. DeWitt, Fundamentals of Heat and Mass Transfer, fifth ed., John Wiley & Sons, 2002.
[47] O. Reynolds, Papers on Mechanical and Physical Subjects, vol. 1, University Press, Cambridge, 1900.
[48] M.J. Vogel, A.H. Hirsa, Concentration measurements downstream of an insoluble monolayer front, J. Fluid Mech. 472 (2002) 283–305.
[49] S. Phongikaroon, K.P. Judd, G.B. Smith, R.A. Handler, The thermal structure of a wind-driven Reynolds ridge, Exp. Fluids 37 (2004) 153–158.
[50] G.L. Gaines Jr., Insoluble Monolayers at Liquid–Gas Interfaces, John Wiley & Sons, New York, NY, 1966.
[51] J.H. Brooks, A.E. Alexander, The spreading behavior and crystalline phases of fatty alcohols, in: Retardation of Evaporation by Monolayers: Transport Processes, Academic Press, 1962, pp. 245–269.
[52] J. Kou, J.R. Saylor, A method for removing surfactants from an air/water interface, Rev. Sci. Instrum. 79 (2008) 123907.
[53] G. Tchobanoglous, F.L. Burton, H.D. Stensel, Wastewater Engineering: Treatment and Reuse, fourth ed., McGraw-Hill, 2002.
[54] R.A. Handler, G.B. Smith, R.I. Leighton, Vortex interactions with a thermal boundary layer at a surfactant contaminated free surface, in: Proceedings of ASME Fluids Engineering Division Summer Meeting, ASME, Washington, DC, 1998.
[55] A.W. Adamson, Physical Chemistry of Surfaces, John Wiley & Sons, New York, NY, 1990.